NASA
Technical Memorandum 101464

AVSCOM
Technical Report 88-C-022

Results of Inphase Axial-Torsional Fatigue Experiments on 304 Stainless Steel

Peter J. Bonacuse
Propulsion Directorate
U.S. Army Aviation Research and Technology Activity—AVSCOM
Lewis Research Center
Cleveland, Ohio

and

Sreeramesh Kalluri
Sverdrup Technology, Inc.
NASA Lewis Research Center Group
Cleveland, Ohio

March 1989

NASA

US ARMY
AVIATION
SYSTEMS COMMAND
AVIATION R&T ACTIVITY

E4576

ERRATA

Results of Inphase Axial-Torsional Fatigue Experiments on 304 Stainless Steel

by

Peter J. Bonacuse and Sreeramesh Kalluri
NASA TM 101464 (AVSCOM TR 88-C-022)
March 1989

Page 11, Appendix : Add the following symbol definitions.
ϵ_{in} Inelastic axial strain amplitude
γ_{in} Inelastic shear strain amplitude

Page 12, Smith-Watson-Topper model: Left hand side of the equation, "$\sigma_1^{max}\ \epsilon_f'/2$" should read as "$\sigma_1^{max}(\Delta\epsilon_1/2)$"

Page 12, Socie's shear and normal strain model : In left hand side of the equation, "$\hat{\epsilon}$" should read as "$\hat{\epsilon}_n$"

Fig. 9 : "KNOPP'S" should read as "KNOOP'S"

Fig. 10(a) : In the Y-axis label, "$\sigma_1^{max}\ \epsilon_f'/2$" should read as "$\sigma_1^{max}(\Delta\epsilon_1/2)$"

Fig. 10(b) : In the Y-axis label, "$\hat{\epsilon}$"should read as"$\hat{\epsilon}_n$"

Fig. 10(c) : "Equivalent strain" should read as as "Equivalent inelastic strain" in two locations

and,

In the Y-axis label,"$MF(\Delta\epsilon_{in}/2)$" should read as "$MF(\Delta\epsilon_{in}/2)_{equ}$"

RESULTS OF INPHASE AXIAL-TORSIONAL FATIGUE EXPERIMENTS ON 304 STAINLESS STEEL

Peter J. Bonacuse
Propulsion Directorate
U.S. Army Aviation Research and Technology Activity - AVSCOM
Lewis Research Center
Cleveland, Ohio 44135

and

Sreeramesh Kalluri
Sverdrup Technology, Inc.
NASA Lewis Research Center Group
Cleveland, Ohio 44135

SUMMARY

A series of axial-torsional, inphase, strain-controlled, low-cycle fatigue tests were performed at room temperature on tubular specimens of 304 stainless steel. The program was conducted in cooperation with the task group on multiaxial fatigue research of ASTM committee E-09. The objective was to quantify the variability in multiaxial test results among several laboratories. This report includes only data generated at the NASA Lewis Research Center's High Temperature Fatigue and Structures Laboratory. The experimental equipment and procedures used are described. The tubular specimens were polished on the outer surface to aid in the use of a cellulose film surface replication technique for crack detection. However, cracking initiated predominantly on the internal surface for all specimens. Honing of the bore of the tubular specimens lessened but did not entirely eliminate this problem. The observed fatigue lives are compared with lives calculated from three multiaxial life models. Constants for the life prediction models were obtained from uniaxial and torsional tests performed on the same heat of material. The observed fatigue lives agreed with calculated lives to within a factor of two for all but one of the life prediction models.

INTRODUCTION

Engineering components are often subjected to multiaxial states of stress due to complex geometries and loading conditions. Fatigue life prediction models that are based solely on uniaxial fatigue data can produce erroneous results if used for the design of components subjected to multiaxial loading. In order to more accurately predict the fatigue life of engine components, researchers will have to develop models by using multiaxial fatigue life data (ref. 1).

Fatigue crack initiation and propagation lifetimes are dependent on the states of stress and strain induced in the material. In uniaxial fatigue tests, cracks usually nucleate at the surface (when no large flaws are present in the interior of the specimen) and propagate into the specimen in mode I fashion (ref. 2). The majority of fatigue testing of engineering alloys is performed on uniaxial test rigs, and the models developed to predict fatigue lives thus are based on uniaxial fatigue data. These life prediction models are therefore biased to mode I type of failure. However, it has been noted by

other investigators (refs. 3 and 4) that when principal stresses are present in multiple directions, as in a torsional test, the mode of crack initiation and propagation can change significantly.

For example, in some materials, many small cracks form on the planes of maximum shear stress and propagate, via mode II, a small distance (less than 0.1 mm) on the surface before they are arrested. Final failure in these materials occurs because of a crack-linking process among the many small cracks. The planes in which crack initiation (growth of cracks to approximately 0.1 mm) occurs have been found to be dependent on the ductility of the material. Ductile materials tend to initiate cracks on maximum shear stress planes (mode II), but brittle materials tend to crack on planes perpendicular to the maximum normal stress (mode I). Some materials, at certain temperatures and stress states, exhibit a transition between the above two types of cracking behavior (ref. 4).

Axial and torsional strains can be applied either inphase (proportional loading) or out-of-phase (nonproportional loading) as shown schematically in figure 1. In inphase tests, the control parameters (axial and torsional strains) peak simultaneously, and the axial control parameter at any given instant is always a product of the torsional control parameter and a constant. In out-of-phase tests, one control parameter lags the other by an arbitrary phase shift (90° is usually recognized as being the worst case in axial-torsional testing). Inphase loading produces principal stresses and strains that have a fixed orientation with respect to the geometry of the specimen; whereas out-of-phase loading causes the directions of the principal stresses and strains to rotate with time. A general multiaxial life prediction theory must take into consideration this non-plane-specific deformation.

These phenomena make it imprudent to predict the lives of components, which seldom see purely uniaxial states of stress and strain in their operating environment, based solely on uniaxial fatigue data.

In the past decade, several investigators have developed multiaxial fatigue testing capabilities with the intention of gaining insight into the damage mechanisms associated with multiaxial fatigue. To date, multiaxial fatigue testing procedures have not been standardized. In order to assess the status of multiaxial fatigue testing capabilities of different laboratories, a round-robin program (a program where identical tests are performed at several laboratories) was organized by the task group on multiaxial fatigue research of ASTM committee E-09. The goal of this program was to establish the ground work for an ASTM standard on multiaxial fatigue testing. Each laboratory in the program was requested to perform room temperature, inphase, axial-torsional fatigue tests on 304 stainless steel at two different strain amplitudes. To monitor crack formation and growth, laboratories were required to perform cellulose film surface replications at specified life intervals.

The results of this round-robin program would also show the extent of variability in the data produced, and the strengths and shortcomings of the various specimen designs and testing equipment.

The results of the inphase axial-torsional fatigue tests conducted in the High Temperature Fatigue and Structures Laboratory of NASA Lewis Research Center are presented in this report. In the discussion section, three different multiaxial life prediction models were utilized to predict the fatigue lives of

the specimens under the prescribed loading conditions. This analysis was performed to compare the predictive capabilities of the models as well as to bound the experimental data. The experience obtained from this small program will be utilized to optimize the specimen design and improve the experimental procedure for future multiaxial fatigue testing at the NASA Lewis Research Center.

EXPERIMENTAL EQUIPMENT

The details of the equipment used for the inphase axial-torsional fatigue tests are presented in the following four subsections: Specimen Geometry and Surface Preparation, Axial-Torsional Load Frame, Extensometry, and Real-Time Test Control and Data Acquisition System. Details of the biaxial testing facilities available in the High Temperature Fatigue and Structures Laboratory of the NASA Lewis Research Center were reported by McGaw and Bartolotta (ref. 5).

Specimen Geometry and Surface Preparation

The geometry of the specimen used in this program is shown in figure 2. The thin-walled tube design has become one of the accepted geometries for multiaxial testing. This design was chosen over the cruciform and bidirectional bending specimens because of its decoupled response, relative lack of strain gradients, and ease of fabrication. A compromise amongst buckling stability, minimization of the radial strain variation, and fabricability has determined the dimensions of the current specimen. The mean diameter of the axial-torsional tubular specimen is about 8 to 10 times larger than the diameters of the specimens used in most uniaxial fatigue tests. The length and cross-sectional area of the axial-torsional tubular specimen are approximately two and five times that of the uniaxial fatigue specimens, respectively.

Tubular fatigue specimens pose problems that are not normally encountered in the testing of solid specimens. Tubular specimens have two surfaces from which cracks can initiate and propagate. Because fatigue is predominantly a surface initiated process (ref. 6), the higher surface-to-volume ratio of a tube can have a detrimental influence on life. Indeed, Ellis (ref. 7), while documenting the results of an interlaboratory uniaxial fatigue test program on alloy 800 H, observed that the fatigue lives obtained with the tubular specimens were lower than those obtained with solid specimens. In addition, during the fabrication process of a tubular specimen, it is difficult to produce a finish on the bore surface which is as good as the finish on the exterior surface.

To address this problem, the original specimen machining instructions specified that the inner surface have a number 8 microfinish. After fabrication, the surface finish of the bore was inspected to ensure that the machining specifications were met. However, because of the limitations of the inspection equipment, it was not possible to measure the internal surface finish at the midsection of the specimen. In fact, even though the internal diameter of the tubular specimen used in this study is fairly large, it is difficult to get a good internal surface finish with conventional mechanical polishing techniques. In the presence of torsional loads, the highest strains occur at the outer surface. Thus, because of the nature of the axial-torsional inphase loading, cracks are more likely to originate at the outer surface of the tubular specimen. This is the case provided that the internal and external surface finishes are of equal quality.

In order to detect small cracks and monitor their propagation with surface replication, the external surfaces of all specimens in the round-robin program were polished to a uniform finish at the University of Illinois at Urbana-Champaign. Internal surfaces were prepared by the individual participants in the program, and hence were not uniform from participant to participant.

Axial-Torsional Load Frame

The MTS 880 load frame used in this program is configured to apply 223 kN in tension and compression and 2.26 kN-m in torsion. The hydraulic collet grips were designed by MTS for a 49.2-mm outer-diameter smooth shank specimen. The gripping pressure is adjustable to material type and loading conditions. The load frame is a standard uniaxial frame that is rated for much higher axial loads but is used in this application for the additional torsional stiffness. The reproducibility of the load train alignment was tested with a strain-gaged specimen. The bending strains were within ASTM recommended standards for axial load frames.

Extensometry

The MTS axial-torsional high-temperature extensometer (model 632.68C-05) was used to measure the axial and torsional strains. The extensometer (fig. 3) has two quartz probes. The top probe is fixed in the tangential direction with respect to the bottom probe and senses only axial displacements, while the bottom probe is fixed in the axial direction with respect to the top probe and senses only tangential (angular) displacements. This arrangement allows the extensometer to move with the rigid body translations of the specimen.

Two indentations were pressed into the specimen's outer surface to prevent the extensometer from slipping. The indentations were placed 25 mm apart within the straight section of the specimen. The depth of the indentations was determined to be important. Indentations that were too shallow would allow the extensometer to slip out at high torsional strains. Indentations pressed too deeply into the specimen caused the interior surface of the specimen to bulge, producing an undesirable, and potentially destabilizing, discontinuity in the specimen geometry. The method currently being used to make the indentations is to press them with an MTS supplied fixture and a mechanical press. A more accurate indenting technique incorporating a displacement controlled fixture is under development. Two spring-loaded cantilever arms acting on the ends of the quartz probes keep the extensometer in contact with the specimen and also support the weight of the extensometer body (fig. 3).

The extensometer was calibrated by MTS and was shown to display less than 1 percent crosstalk between the axial and torsional strain measurements. Calibration was verified before and after the round-robin program was conducted and was found to be within acceptable limits. The extensometer is capable of measuring ±10.0 percent axial strain and ±4.2 percent shear strain (equivalent to a twist amplitude of 5° within a 25-mm gage section).

Real-Time Test Control and Data Acquisition System

A Data General S/20 computer system interfaced to digital-to-analog (D/A) and analog-to-digital (A/D) converters was used to generate the servocontroller command waveform and acquire data from the axial and torsional load, strain, and stroke transducers. Data on all six channels were acquired at 500 points per cycle. Data were collected continuously during the first 10 cycles and at logarithmic intervals thereafter. Specifications of the computer systems and peripheral hardware are shown in table I. The test control software was written in Pascal with device driver procedures written in assembler. The software takes advantage of the multitasking abilities of the S/20 computer to output data to hard disk storage and perform test control functions simultaneously.

EXPERIMENTAL PROCEDURE

The experimental test matrix was prepared by the organizers of the round-robin program. Two inphase axial-torsional fatigue tests of different strain amplitudes were specified. Two additional tests, duplicating the strain conditions of the prescribed tests, were also performed without any pauses for surface replication. All the experiments were conducted at room temperature in air under strain control. The material selected for the program by the ASTM task group was AISI 304 stainless steel. It was chosen because of the relatively large quantity of multiaxial fatigue data that existed for an available heat of this material. The material for the round-robin program was supplied by the University of Illinois at Urbana-Champaign. The chemical composition of the 304 stainless steel is shown in table II.

At the beginning of each test, a procedure was used to gradually increase the completely reversed ($R = -1$) amplitude of the sine wave over five cycles to the required matrix strain amplitude. These five cycles were not counted in the life of the specimen, and no data were collected during these cycles.

Test Matrix

The test matrix used in this study is shown in table III. The frequencies allowed by the round-robin program ranged from 0.1 to 1.0 Hz. It was determined, particularly in the high-strain regime, that the heat generation due to plastic work would cause experimental difficulties. When the specimen was cycled at the higher strain amplitude at a frequency of 0.5 Hz, the steady-state temperature of the specimen rose over 100 °C. With the frequency reduced to the lowest allowable value of 0.1 Hz, the temperature still rose over 40 °C. These temperature increases do not significantly effect the bulk properties of the material, but they did cause a thermal expansion/contraction problem during the zero stress/zero strain surface replication pauses. During the pause the specimen would cool and the servocontroller (under strain control) would compensate for the thermal strain by increasing the tensile load. After cycling the specimen for 500 cycles at the higher strain amplitudes of the test matrix with a frequency of 0.5 Hz, the tensile stress during the surface replication pause approached 297 MPa, an unacceptably high value. To avoid this problem the tests were all run at the lowest allowable frequency (0.1 Hz), and a procedure was added to the test control software which held the axial strain at zero until the specimen cooled and then deformed the specimen plastically to reach a zero load, zero strain condition.

Surface Replication

As specified by the round-robin organizers (table III), surface replicas were taken every 5000 cycles for the lower strain amplitude test and every 500 cycles in the higher strain amplitude test. No surface replication was performed in the duplicate tests, so no pauses were required. Because the extensometer and its fixturing would not allow the complete gage section to be replicated, they were removed at each replication pause. Acetyl cellulose film (0.034 mm thick) applied with acetone was used to record the topography of the specimen's outer surface. Four replicas were taken around the gage section. Each replica was approximately 1.5 by 2 in. so that there was some overlap in replication. Reference marks, etched on the shoulder of the specimen prior to its installation in the grips, were used to record the orientation and position of each replica.

EXPERIMENTAL RESULTS

Fatigue Lives and the Nature of Hysteresis Loops

The lower strain amplitude (0.25 percent axial and 0.433 percent torsional) test was interrupted at 5000 cycle intervals and replicas of the external surface were taken. Examination of the replicas and of the specimen surface at each interval showed no apparent cracking. The specimen failed because of an internal crack at 23 278 cycles (four surface replications). The higher strain amplitude test (0.6 percent axial and 1.0 percent torsional) was interrupted after every 500 cycles to replicate the surface. This specimen failed after 1971 cycles (three surface replications). Again, at each interval no external cracking was observed in either the replicas or the specimen. Duplicates of each test, which were not paused for surface replication, failed at 36 086 and 2081 cycles respectively. The final failure crack in all cases was large enough to cause the extensometer to slip out of the indentations. When this occurred a preset electronic limit was tripped and the hydraulics were shut down. Efforts are being made to introduce additional programmed limits in the software. These software limits will be sensitive to rates of peak load dropoff and will allow tests to be shut down soon after the development of a sizable crack in the specimen. The software limits will also prevent the slippage of the extensometer from the indentation as the specimen begins to fail, thus preventing possible damage to the extensometer. Inphase axial-torsional fatigue data generated in this program are shown in table IV.

The high- and low-strain-amplitude hysteresis loops for the interrupted tests are presented in figures 4 and 5. Axial and torsional data are presented for the following three cases: (1) beginning of test, (2) near half-life, and (3) near end of test.

These hysteresis loops show some unusual material behavior. Shear stress in the torsional hysteresis loops of the higher strain amplitude test exhibited a small reduction near the peak torsional strains. To verify whether this phenomenon was due to a material-induced coupling between the axial and torsional deformations, the higher strain test was conducted on another specimen with only the torsional deformation imposed. This test showed no flattening or dropoff of the torsional stress as the strain approached its peak values. Four additional verification tests were run, each with an increased amount of proportional axial strain superimposed on the full amplitude torsional strain.

Each time the axial strain was incremented, the specimen was allowed to stabilize over 20 to 30 cycles. This was done to remove the effect of transient isotropic hardening. The flattening of the torsional loop in these tests was proportional to the amount of axial strain imposed. This seems to indicate that the imposed axial stress allows the material to flow more readily in the torsional direction.

In von Mises equivalent stress/strain space one would expect the yield and plastic flow behavior to be similar to the pure shear condition for an initially isotropic material (ref. 8). This qualitatively explains why the torsional loop flattens with the addition of an inphase axial deformation, but it does not explain the small drop in torsional stress near the peak. Further experimentation and analysis are required to determine how much of the flattening of the torsional loop is due to kinematic translation and/or rotation of the yield surface and how much of this flattening, if any, is due to extrusion-induced anisotropy imparted in the fabrication of the bar stock.

Metallographic studies were performed on an undeformed specimen to determine the extent of work hardening and to document the microstructure of the gage section. A micrograph of the longitudinal section of an undeformed specimen (fig. 6) clearly shows stringers along the direction of extrusion. Similar stringers from the same heat of material were identified with Auger analysis as manganese sulfide by Bannantine (ref. 9). However, x-ray energy dispersion spectra studies on the stringers failed to reveal either Mn or S in this phase. In order to determine the phase of the stringers, an additional metallographic examination of the same longitudinal section was conducted with a modified Murakami's etchant proposed by Burgess and Forgeng (ref. 10). This etchant reveals sigma phase as light blue and ferrite as yellow. Carbides are not attacked by this etchant. As can be seen in the enlarged view of the longitudinal section (fig. 7), the stringers are etched yellow indicating that they are elongated ferrite grains. These elongated ferrite grains support the theory that there may be some extrusion-induced anisotropy.

In all the tests, as the specimen approached failure, both the axial and torsional hysteresis loops exhibited the dogleg behavior characteristic of the presence of a dominant crack.

Stress versus Life Curves

The plots of axial stress and torsional stress versus cycles are depicted in figure 8 for the two strain amplitudes. The continuous (uninterrupted) tests are plotted along with the interrupted experiments. The stress amplitude versus applied cycles curves for all tests show some initial hardening followed by cyclic softening which continued until failure. More softening was observed in the axial data than in the torsional data for both strain amplitudes.

Failure Modes

Failure occurred because of a single dominant crack in all specimens. The final failure crack always initiated on the internal surface. External surface replication proved to be fruitless because no external cracks were detectable until final failure. In the interrupted tests (no honing), the internal cracks (which were numerous, particularly in the low-strain regime) initiated at circumferential machining marks left by the boring operation.

The dominant crack propagated by linking up with the multitude of smaller cracks. To alleviate this problem, the internal surface of the specimens used for the uninterrupted tests was honed to a number 8 microfinish. Cracks still formed preferentially on the internal surface at the small machining marks left by the honing process (45° to the specimen axis). In all cases, regardless of the orientation of the initial crack, the dominant crack propagated perpendicular to the maximum normal stress direction (approximately 60° from the specimen axis).

DISCUSSION

Experimental Results

The uninterrupted tests show a somewhat smaller amount of axial hardening than the tests interrupted for surface replication (fig. 8). The difference in hardening behavior of honed versus unhoned specimens might be due to the degree of work hardening of the surfaces. Microhardness tests were performed on a bored specimen to determine variation in hardness in the gage section of an undeformed specimen. A section from the grip of the same specimen was also tested to obtain a reference hardness. The gage section exhibited higher hardness values near the inner and outer surfaces than at the center. Higher average hardness was also observed in the gage section compared to the grip section (fig. 9). Honing may have reduced the average initial hardness by removing some of the previously work hardened material.

In the duplicate (uninterrupted) tests, two variables were changed with respect to the interrupted experiments. First, the bores of the tubular specimens were honed to improve the internal surface finish. In addition, the experiments were not interrupted for the purpose of external surface replication. As a result, it was not necessary to dismount and reseat the extensometer. These changes could affect (either increase or decrease) the fatigue life of the specimen. As observed in table IV, the uninterrupted inphase axial-torsional fatigue life improved significantly in the high-cycle regime while improvement of fatigue life in the low-cycle regime was marginal. Errors in reseating the extensometer probes in the indentations after each surface replication could also have affected the fatigue life of the interrupted axial-torsional experiments by inducing a small amount of inadvertent mean strain. However, the effect of extensometer-removal-induced mean strains on fatigue life is not likely to be of the same order as the effect of honing.

Comparison of Observed Fatigue Lives to Those Predicted by Multiaxial Fatigue Life Models

The room-temperature axial, torsional, and axial-torsional fatigue properties of the heat of 304 stainless steel used in the current program were well characterized at the University of Illinois (refs. 4 and 9). Experimentally observed inphase axial-torsional fatigue lives in the current program were compared with the predictions of three multiaxial fatigue life estimation models by using the 304 stainless steel material constants reported by Bannantine (ref. 9).

Two of the models used for comparison were (1) a modified Smith-Watson-Topper (SWT) model (refs. 4 and 11) and (2) Socie's model (ref. 4). The latter

model takes into consideration the maximum shear strain, the stress normal to the plane of maximum shear, and the mean stress in estimating the fatigue life under multiaxial conditions. In the development of these two models (and their associated constants), failure was defined as the initiation and growth of an external surface crack to a length of 1 mm. Because the definition of failure for the experiments reported here is based on a longer crack length (10 to 15 mm), the predicted lives are likely to be on the conservative (lower life) side. A third model proposed by Manson and Halford (ref. 12) in their discussion of a paper by Zamrik et al. (ref. 13) was also used to estimate the inphase axial-torsional fatigue lives. This model modifies the equivalent inelastic strain by a multiaxiality factor. The equations for all three models are presented in the appendix.

Graphs of the multiaxial life prediction models and the fatigue data generated in this program are shown in fig. 10. The observed and predicted fatigue lives also appear in table V. In most cases the fatigue lives observed in this program were lower than the predictions of the models. This is contrary to the expectation stated for the modified SWT and Socie models. However, it is not altogether surprising since, in the current program, most of the cracking initiated on the internal surfaces of the tubular specimens.

At this stage, it is difficult to quantify the extent of reduction of fatigue life due to internal cracking. However, some indication can be obtained from the literature. Bannantine (ref. 9), while testing 304 stainless steel in axial-torsional fatigue, observed multiple cracks on the external surface long before the tubular specimen failed. In our experiments no cracks were observed on the outer surface prior to failure. Thus, premature cracking due to flaws in the internal surface finish could have reduced the observed fatigue lives in the current program. Overpredictions of the fatigue lives by Socie's shear strain parameter were larger than for the other models. This is due to the fact that Socie's model was developed for materials that exhibit shear crack failure whereas 304 stainless steel fails predominantly on planes perpendicular to the maximum tensile stress direction (ref. 9).

The fatigue lives observed are opposite to the trend that is expected from the difference in the definitions of failure of the specimen. The difference in failure definition between the two programs should not have a large effect on the reported fatigue lives. Because the axial and torsional loads did not drop off until the last several cycles of each test it can be inferred that the final failure crack propagated the majority of its length only in the last fraction of a percent of the life.

CONCLUSIONS

The following conclusions were drawn from the results of the inphase axial-torsional fatigue experiments on 304 stainless steel.

1. The inphase axial-torsional fatigue lives predicted by the multiaxial fatigue life prediction models were higher by a factor of two than those observed in this part of the round-robin program except for Socie's model, the predictions of which were higher by a factor of three. The models predicted higher lives than those observed probably because of premature cracking at the inner surface of the tubular specimen.

2. External surface replications taken in this study provided no useful information because all of the tubular specimens failed due to internal cracking.

3. Among the three different multiaxial fatigue life prediction models used for comparing the experimental and predicted fatigue lives, the predictions by the Manson-Halford model and the Smith-Watson-Topper model were closer to the experimental results than those obtained by the Socie shear strain model. This is attributable to the tensile mode of failure exhibited by 304 stainless steel at room temperature and the tensile mode of failure emphasized by the Manson-Halford and Smith-Watson-Topper models.

4. The premature failure of tubular specimens due to crack initiation at the inner surface can be minimized by honing the bore of the tubular specimen. Honing improved the fatigue life to a greater extent in the high-cycle fatigue region than in the low-cycle fatigue region.

5. Metallographic studies of the specimen revealed the presence of ferrite stringers along the axis of the tubular specimens. The orientation of these stringers indicates that there might be some extrusion-induced anisotropy in the material. Such microstructure-related anisotropy could be responsible for the observed flattening of the torsional hysteresis loops near the peak loads. The extent to which this microstructural anisotropy affects the deformation behavior of this material is as yet uncharacterized.

APPENDIX - MULTIAXIAL FATIGUE LIFE PREDICTION MODELS

This appendix contains the functional forms of the three models presented in the discussion section of this paper.

Symbols

b_a	axial fatigue strength exponent, -0.114
b_t	torsional fatigue strength exponent, -0.121
c_a	axial fatigue ductility exponent, -0.402
c_t	torsional fatigue ductility exponent, -0.353
E	elastic modulus, 185 GPa
G	shear modulus, 82.8 GPa
MF	multiaxiality factor
TF	triaxiality factor
$\hat{\gamma}$	maximum shear strain amplitude
γ'_f	shear fatigue ductility coefficient, 0.315
$\left[\frac{\Delta\varepsilon_{in}}{2}\right]_{equ}$	equivalent inelastic strain amplitude
$\Delta\varepsilon_1$	first principal strainrange
ε'_f	tensile fatigue ductility coefficient, 0.171
$\hat{\varepsilon}_n$	tensile strain perpendicular to maximum shear strain amplitude
σ'_f	tensile fatigue strength coefficient, 1000 MPa
$\hat{\sigma}_{no}$	mean stress perpendicular to maximum shear strain amplitude
σ_1^{max}	maximum principal stress
τ'_f	shear fatigue strength coefficient, 709 MPa
$2N_f$	reversals to formation of a 1.0-mm crack

The parameter values given here are derived from the room-temperature fatigue tests performed at the University of Illinois on 304 stainless steel (ref. 9).

Smith-Watson-Topper Model (refs. 4 and 11)

$$\sigma_1^{max} \frac{\varepsilon_f'}{2} = \sigma_f'\varepsilon_f'(2N_f)^{(b_a+c_a)} + \frac{\sigma_f'^2}{E}(2N_f)^{2b_a}$$

Socie's Shear and Normal Strain Model (ref. 4)

$$\hat{\gamma} + \hat{\varepsilon} + \frac{\hat{\sigma}_{no}}{E} = \gamma_f'(2N_f)^{c_t} + \frac{\tau_f'}{G}(2N_f)^{b_t}$$

Manson and Halford's Modified Equivalent Strain Model (ref. 12)

$$MF\left[\frac{\Delta\varepsilon_{in}}{2}\right]_{equ} = \varepsilon_f'(2N_f)^{c_a}$$

where

$$\left[\frac{\Delta\varepsilon_{in}}{2}\right]_{equ} = \left\{\varepsilon_{in}^2 + \frac{\gamma_{in}^2}{3}\right\}^{1/2}$$

$$MF = \frac{1}{2 - TF} \quad \text{for} \quad TF \leq 1$$

$$MF = TF \quad \text{for} \quad TF \geq 1$$

and

$$TF = \frac{\sigma_1 + \sigma_2 + \sigma_3}{\frac{1}{\sqrt{2}}\sqrt{(\sigma_1 - \sigma_2)^2 + (\sigma_2 - \sigma_3)^2 + (\sigma_3 - \sigma_1)^2}}$$

where σ_1, σ_2, and σ_3 are principal stresses and $\sigma_1 > \sigma_2 > \sigma_3$.

REFERENCES

1. Garud, Y.S.: Multiaxial Fatigue: A Survey of the State of the Art. J. Test. Eval., vol. 9, no. 3, May 1981, pp. 165-178.

2. Dowling, N.E.: Crack Growth During Low-Cycle Fatigue of Smooth Axial Specimens. Cyclic Stress-Strain and Plastic Deformation Aspects of Fatigue Crack Growth, ASTM STP-637, ASTM, 1977, pp. 97-121.

3. Brown, M.W; and Miller, K.J.: A Theory for Fatigue Failure Under Multiaxial Stress-Strain Conditions. Proc. Inst. Mech. Eng., vol. 187, no. 65/73, 1973, pp. 745-755.

4. Socie, D.F.: Multiaxial Fatigue Damage Models. J. Eng. Mater. Technol., vol. 109, no. 4, 1987, pp. 293-298.

5. McGaw, M.A.; and Bartolotta, P.A.: The NASA Lewis Research Center High Temperature Fatigue and Structures Laboratory. 4th Annual Hostile Environments and High Temperature Measurements Conference Proceedings, Society for Experimental Mechanics, 1987, pp. 12-29.

6. Fuchs, H.O; and Stephens, R.I.: Metal Fatigue in Engineering. John Wiley and Sons, 1980, p. 29.

7. Ellis, J.R.: Results of an Interlaboratory Fatigue Test Program Conducted on Alloy 800H at Room and Elevated Temperatures. NASA CR-174940, 1985.

8. Mendelson, A.: Plasticity: Theory and Application. Macmillan, 1968, pp. 116-119.

9. Bannantine, J.A.: Observations of Tension and Torsion Fatigue Cracking Behavior and the Effect on Multiaxial Damage Correlations. M.S. Thesis, University of Illinois at Urbana-Champaign, 1986. (UILU-ENG-86-3605, Report 128).

10. Vander Voort, G.F.: Metallography Principles and Practice. McGraw-Hill, 1984, pp. 647-652.

11. Smith, K.N.; Watson, P; and Topper, T.H.: A Stress-Strain Function for the Fatigue of Metals. J. Mater., vol. 5, no. 4, Dec. 1970, pp. 767-778.

12. Manson, S.S.; and Halford, G.R.: Multiaxial Low-Cycle Fatigue of Type 304 Stainless Steel. J. Eng. Mater. Technol., vol. 99, no. 3, July 1977, pp. 283-285.

13. Blass, J.J.; and Zamrik, S.Y.: Multiaxial Low-Cycle Fatigue of Type 304 Stainless Steel. 1976 ASME-MPC Symposium on Creep-Fatigue Interaction, R.M. Curran, ed., ASME, 1976, pp. 129-159.

TABLE I. - SPECIFICATIONS FOR THE COMPUTER SYSTEMS AND PERIPHERAL HARDWARE

(a) 16-bit minicomputer (Data General S/20 computer)

Cycle time, ns	500
RAM, kbytes	512
Disk	
Type	Winchester
Capacity, Mbytes	5
Drive	
Type	Floppy
Capacity, Mbytes	1.2

(b) Digital-to-analog converter

Resolution, bits	12
Conversion time, μsec	7
Number of channels	2

(c) Analog-to-digital converter and multiplexer

Resolution, bits	12
Number of channels	16
Multiplexer switching time, μsec	10
Conversion time, μsec	7
Aperture, μsec	5

TABLE II. - CHEMICAL COMPOSITION OF AISI 304 STAINLESS STEEL

[From ref. 9.]

Element	Composition, wt %
Chromium	19.2
Nickel	10.8
Manganese	1.6
Silicon	.4
Carbon	.057
Sulfur	.023
Phosphorus	<.01
Iron	Balance

TABLE III. - TEST MATRIX

Axial strain amplitude	Torsional strain amplitude	Number of cycles for surface replication	Number of tests required
0.00250	0.00433	500	1
.00600	.01000	5000	1

TABLE IV. - INPHASE AXIAL-TORSIONAL FATIGUE DATA

[Material, 304 stainless steel; frequency, 0.1 Hz.]

Specimen number	Finish of inside surface	Axial strain amplitude, ε	Torsional strain amplitude, γ	Axial stress amplitude, σ, MPa	Axial mean stress, σ_0, MPa	Torsional stress amplitude, τ, MPa	Torsional mean stress, τ_0, MPa	Cycles to failure, N_f
SS-3	Bored[a]	0.00247	0.00428	194	-5.0	108	11.8	23 278
SS-5	Bored[a]	.00597	.00991	301	2.3	152	-1.3	1 971
SS-4	Honed[b]	.00248	.00428	184	-2.0	108	3.0	36 086
SS-6	Honed[b]	.00598	.00992	297	-5.0	151	1.3	2 081

[a]Paused for surface replication.
[b]Continuous test without surface replication.

TABLE V. - OBSERVED AND PREDICTED REVERSALS TO FAILURE

Specimen number	Finish of inside surface	Observed number of reversals to failure, $2N_f$	Predicted number of reversals to failure, $2N_f$		
			Smith-Watson Topper model	Socie's model	Manson and Halford's model
SS-3	Bored	46 556	122 808	196 700	59 886
SS-5	Bored	3 942	5 307	10 760	4 460
SS-4	Honed	72 172	138 379	194 490	57 633
SS-6	Honed	4 162	5 430	10 857	5 433

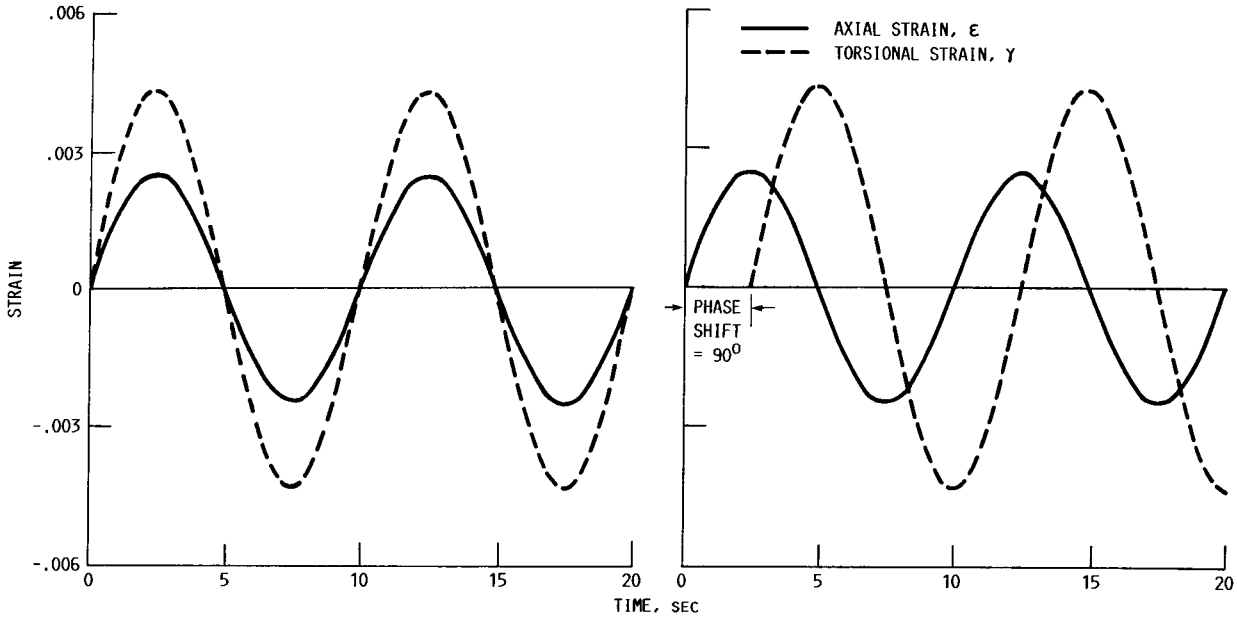

(a) AXIAL-TORSIONAL INPHASE LOADING. (b) AXIAL-TORSIONAL OUT-OF-PHASE LOADING.

FIGURE 1. - INPHASE AND OUT-OF-PHASE AXIAL-TORSIONAL WAVEFORMS.

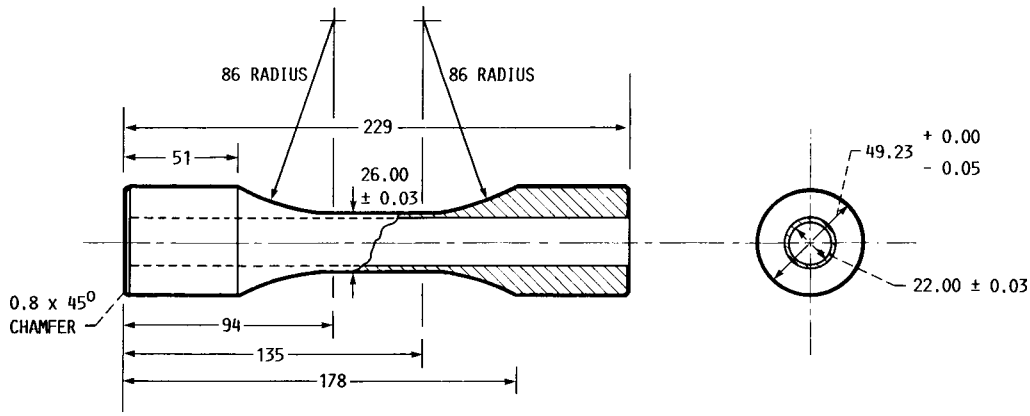

FIGURE 2. - TUBULAR AXIAL-TORSIONAL FATIGUE SPECIMEN. ALL DIMENSIONS ARE GIVEN IN MILLIMETERS.

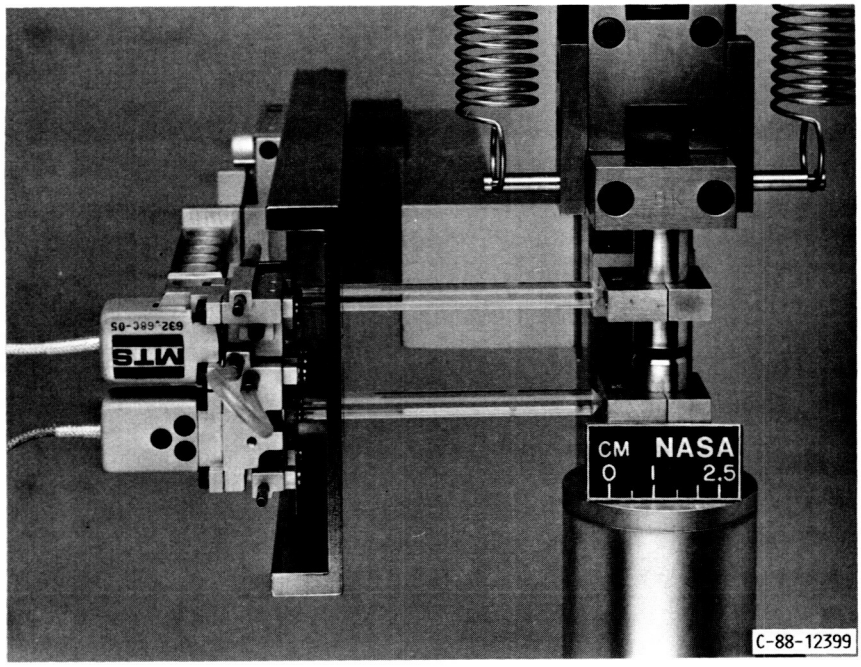

FIGURE 3. - AXIAL-TORSIONAL EXTENSOMETER.

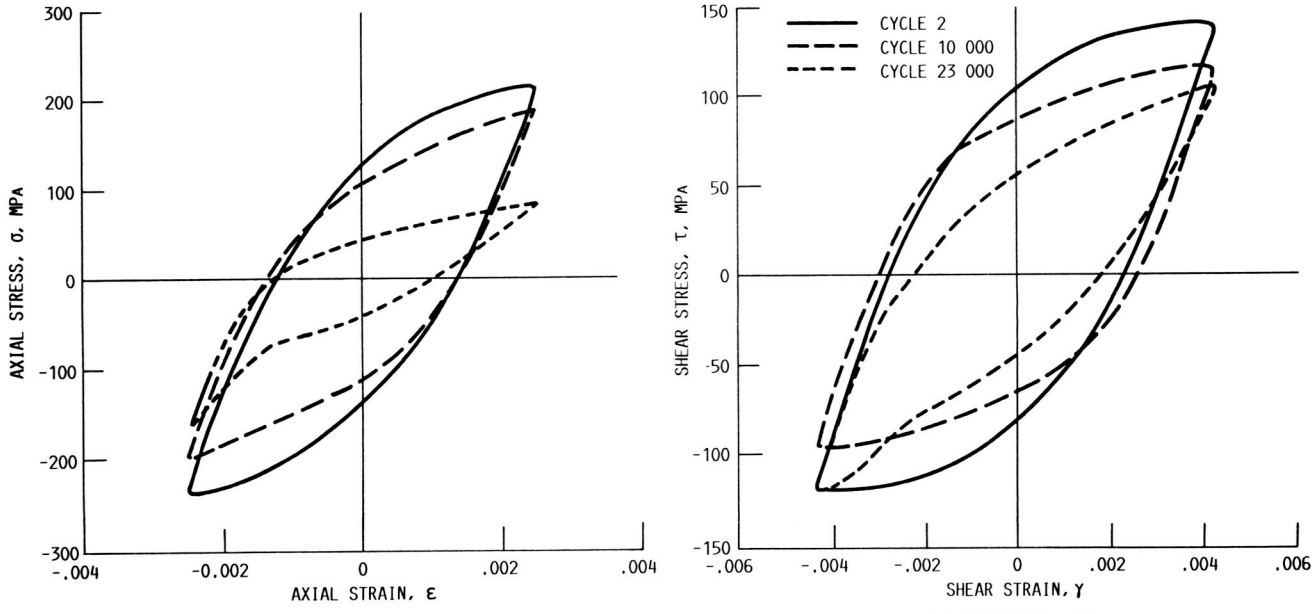

(a) AXIAL LOOP.

(b) TORSIONAL LOOP.

FIGURE 4. - LOW-STRAIN AMPLITUDE HYSTERESIS LOOPS OF INTERRUPTED INPHASE AXIAL-TORSIONAL FATIGUE TESTS.

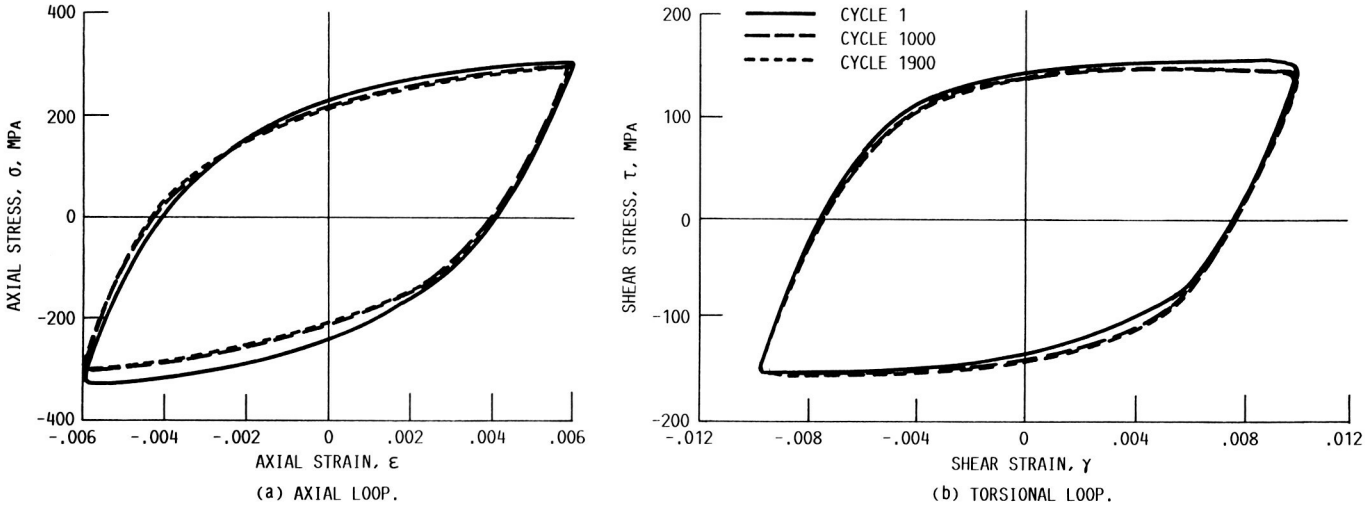

(a) AXIAL LOOP.

(b) TORSIONAL LOOP.

FIGURE 5. - HIGH-STRAIN AMPLITUDE HYSTERESIS LOOPS OF INTERRUPTED INPHASE AXIAL-TORSIONAL FATIGUE TESTS.

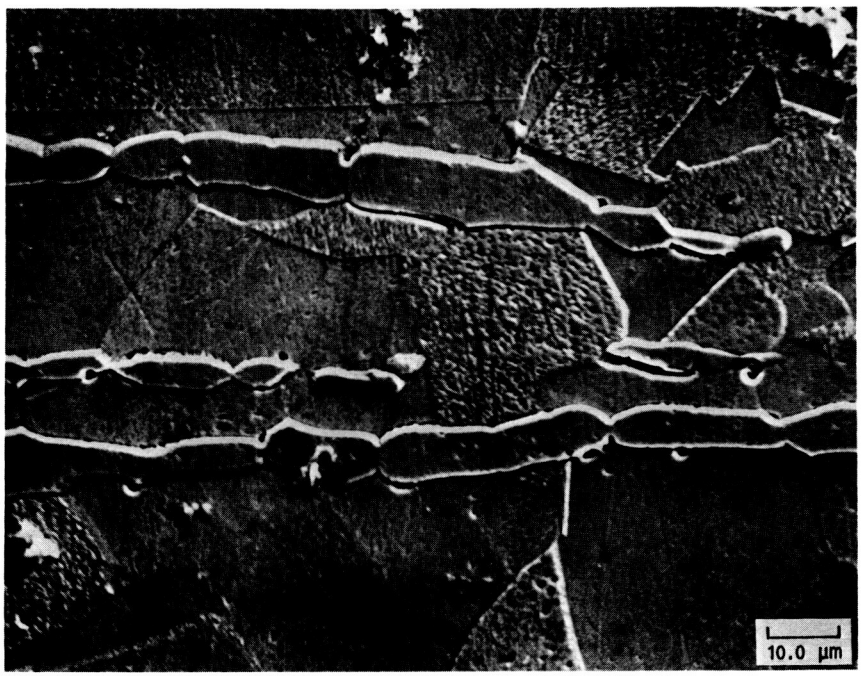

FIGURE 6. - MICROSTRUCTURE OF AISI 304 STAINLESS STEEL. THE ELONGATED FERRITE GRAINS FOLLOW THE EXTRUSION DIRECTION OF THE BAR. ETCHANT, 10 PERCENT OXALIC ACID.

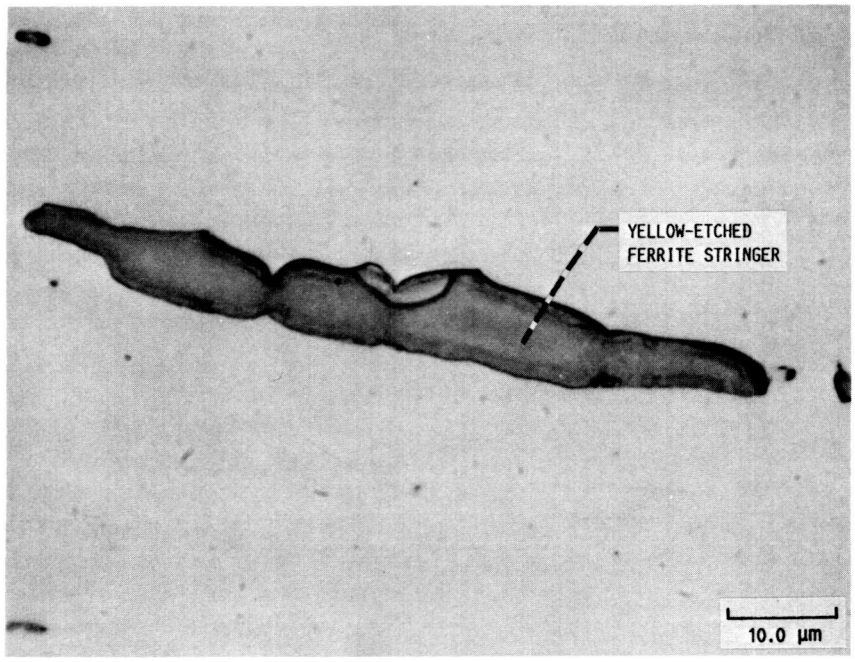

FIGURE 7. - ENLARGED VIEW OF THE FERRITE STRINGER. ETCHANT, MODIFIED MURAKAMI'S REAGENT.

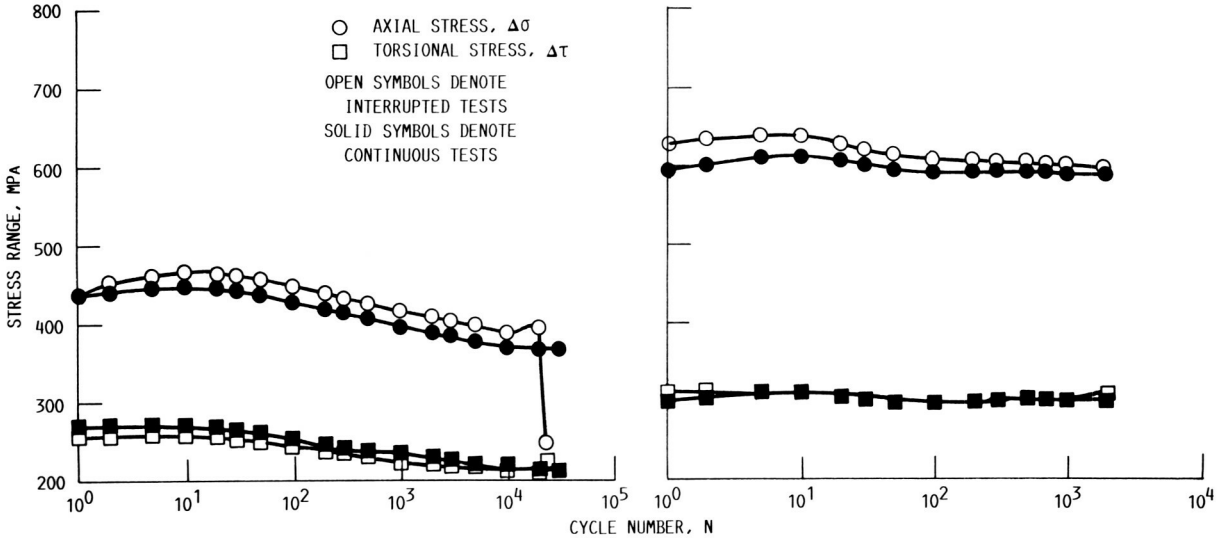

(a) LOW-STRAIN TESTS. (b) HIGH-STRAIN TESTS.

FIGURE 8. - STRESS RANGE VERSUS NUMBER OF CYCLES.

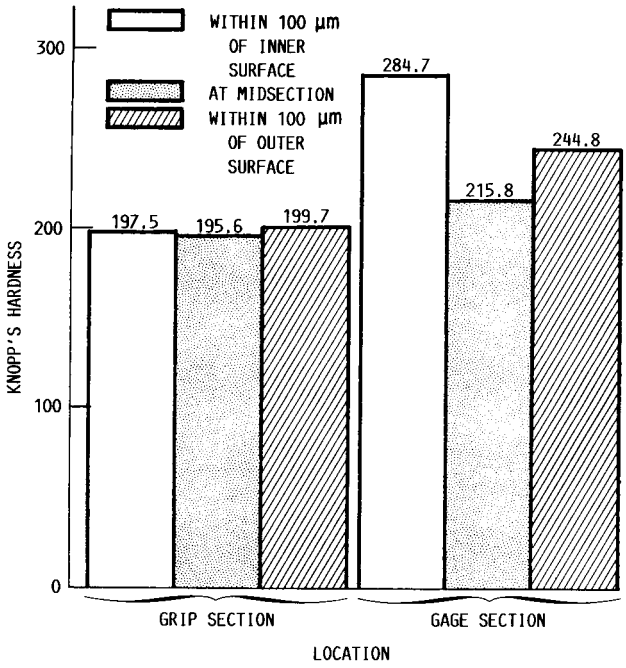

FIGURE 9. - HARDNESS MEASUREMENTS TAKEN IN AN UNDEFORMED AXIAL-TORSIONAL TUBULAR SPECIMEN AT SEVERAL LOCATIONS; MATERIAL, 304 STAINLESS STEEL, EACH BAR REPRESENTS AN AVERAGE OF TEN MEASUREMENTS.

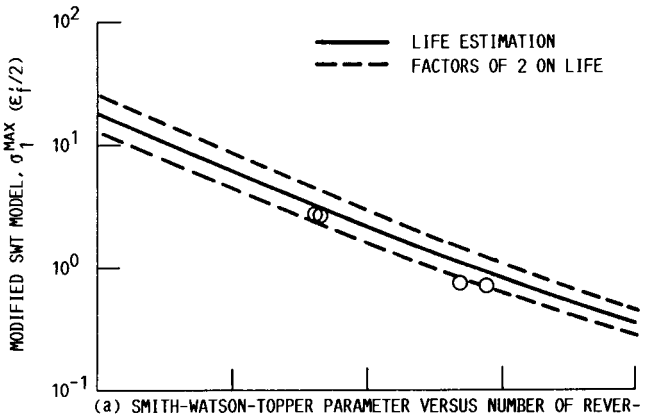

(a) SMITH-WATSON-TOPPER PARAMETER VERSUS NUMBER OF REVERSALS TO FAILURE.

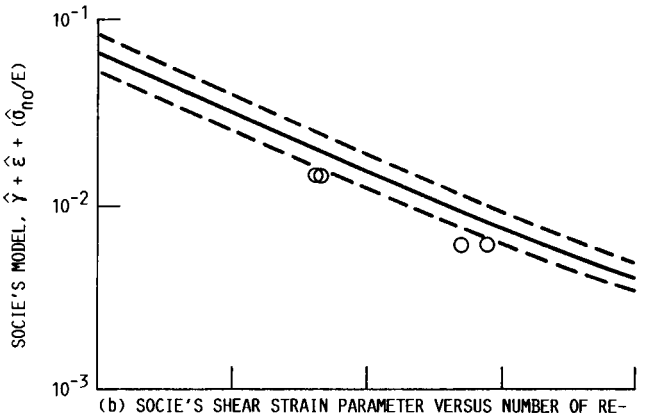

(b) SOCIE'S SHEAR STRAIN PARAMETER VERSUS NUMBER OF REVERSALS TO FAILURE.

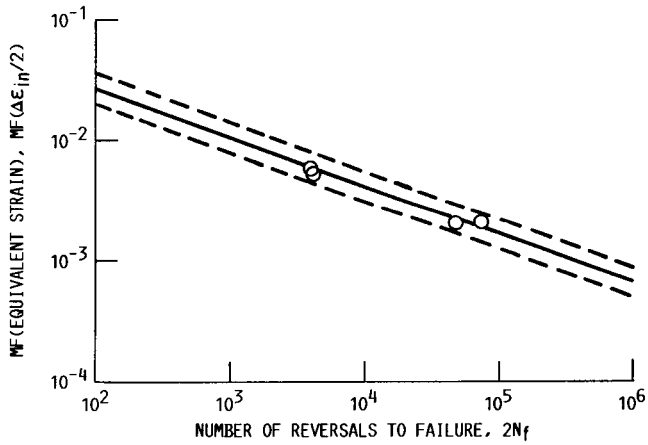

(c) MANSON-HALFORD MULTIAXIALITY FACTOR (MF) TIMES EQUIVALENT STRAIN AMPLITUDE VERSUS NUMBER OF REVERSALS TO FAILURE.

FIGURE 10. - ESTIMATION OF CYCLIC LIVES FOR INPHASE AXIAL-TORSIONAL FATIGUE TESTS WITH THREE LIFE MODELS.

NASA
National Aeronautics and Space Administration

Report Documentation Page

1. Report No.	2. Government Accession No.	3. Recipient's Catalog No.
NASA TM-101464 AVSCOM TR-88-C-022		

4. Title and Subtitle	5. Report Date
Results of Inphase Axial-Torsional Fatigue Experiments on 304 Stainless Steel	March 1989
	6. Performing Organization Code

7. Author(s)	8. Performing Organization Report No.
Peter J. Bonacuse and Sreeramesh Kalluri	E-4576
	10. Work Unit No. 505-63-1B

9. Performing Organization Name and Address	11. Contract or Grant No.
NASA Lewis Research Center Cleveland, Ohio 44135-3191 and Propulsion Directorate U.S. Army Aviation Research and Technology Activity—AVSCOM Cleveland, Ohio 44135-3127	
	13. Type of Report and Period Covered Technical Memorandum

12. Sponsoring Agency Name and Address	14. Sponsoring Agency Code
National Aeronautics and Space Administration Washington, D.C. 20546-0001 and U.S. Army Aviation Systems Command St. Louis, Mo. 63120-1798	

15. Supplementary Notes

Peter J. Bonacuse, Propulsion Directorate; Sreeramesh Kalluri, Sverdrup Technology, Inc., NASA Lewis Research Center Group, Cleveland, Ohio 44135.

16. Abstract

A series of axial-torsional, inphase, strain-controlled, low-cycle fatigue tests were performed at room temperature on tubular specimens of 304 stainless steel. The program was conducted in cooperation with the task group on multiaxial fatigue research of ASTM committee E-09. The objective was to quantify the variability in multiaxial test results among several laboratories. This report includes only data generated at the NASA Lewis Research Center's High Temperature Fatigue and Structures Laboratory. The experimental equipment and procedures used are described. The tubular specimens were polished on the outer surface to aid in the use of a cellulose film surface replication technique for crack detection. However, cracking initiated predominantly on the internal surface for all specimens. Honing of the bore of the tubular specimens lessened but did not entirely eliminate this problem. The observed fatigue lives are compared with lives calculated from three multiaxial life models. Constants for the life prediction models were obtained from uniaxial and torsional tests performed on the same heat of material. The observed fatigue lives agreed with calculated lives to within a factor of two for all but one of the life prediction models.

17. Key Words (Suggested by Author(s))	18. Distribution Statement
Fatigue; Life prediction; Axial-torsional inphase experiments; Hysteresis loops; Stainless steel	Unclassified – Unlimited Subject Category 39

19. Security Classif. (of this report)	20. Security Classif. (of this page)	21. No of pages	22. Price*
Unclassified	Unclassified	20	A03

*For sale by the National Technical Information Service, Springfield, Virginia 22161